A Comparison of Indoor MIMO Measurements and Ray-Tracing at 24 GHz and 2.55 GHz

Jon W. Wallace *Senior Member, IEEE,* Waseh Ahmad, Yahan Yang, Rashid Mehmood, *Member, IEEE,* Michael A. Jensen *Fellow, IEEE,*

***Abstract*—Co-located 4×4 multiple-input multiple-output (MIMO) measurements at 2.55 and 24 GHz are presented for two university buildings consisting of classrooms and offices. Link gain in hallways and connected labs looks similar at the two frequencies when the effect of lower effective receive antenna aperture with increasing frequency is removed. Non-line-of-sight (NLOS) propagation through a wall or around hallway corners exhibits approximately 5-20 dB (11 dB on average) greater loss beyond the 20 dB aperture loss at 24 GHz compared to that at 2.55 GHz. Fixed directional antennas increase path loss by an average of 13 dB when misaligned. Capacity for normalized signal-to-noise ratio is very similar in the two bands and is close to that for the optimal i.i.d. case, indicating sufficient multipath for spatial multiplexing at 24 GHz. A ray-tracing study suggests that material loss must increase from 2.55 GHz to 24 GHz to correctly predict the higher path loss at 24 GHz in severely obstructed scenarios, indicating a need for future material characterization in high microwave bands. The results suggest that 24 GHz is a viable option to replace medium-range (10-30 m) NLOS wireless services currently operating at 2.4 GHz.**

***Index Terms*—Radio propagation, MIMO systems, Multipath channels**

I. Introduction

THE AVAILABILITY of wireless devices operating in the lower-frequency UHF and microwave bands has increased significantly in the last decade, which has dramatically improved the breadth of services available to consumers and industry. Unfortunately, the limited available wireless spectrum coupled with the dramatic growth in the user base has widened the gap between the data rate offered by wireless services and that available in wired networks. For example, only 80 MHz of bandwidth is available to support the 2.4 GHz band, which has become the de facto standard for wireless computer networking. While peak transmission rates for WiFi have steadily increased through exploitation of higher order modulation, diversity, beamforming, and multiple-input multiple-output (MIMO) signaling with current peak rates of 600 Mb/s in a 40 MHz channel, achieved rates of 50-100 Mb/s [1, 2] are more typical. In contrast, gigabit ethernet (GbE) is standard in most wired network installations, with 10 Gb/s GbE becoming increasingly common. Similarly, in cellular networks, 4G LTE supports typical data transmission rates in the modest range of 10 to 50 Mb/s [3, 4], far short of the desired gigabit wireless throughputs that have become an important aim of 5G networks.

Motivated by the desire to increase wireless throughputs despite limited available spectrum in traditional bands, significant effort has focused on exploring the use of millimeter-wave (mm-wave) bands from 30-300 GHz – where significantly more spectrum is available – for wireless services. For example, considerable work has focused on achieving multi-gigabit speeds using the 7 GHz of bandwidth available near 60 GHz (57-64 GHz[1]). But channel measurements show that radio propagation in these bands suffers from high attenuation [5–13], suggesting that line-of-sight (LOS) radio conditions may be necessary for reliable operation near 60 GHz. Furthermore, studies that focus on the directional properties of the propagation channel [14, 15] confirm high reflection and transmission losses, indicating that directional antennas may be needed and that multipath may be insufficient for MIMO signaling. Additionally, the cost of semiconductor devices operating at 60 GHz is relatively high compared to that of UHF and microwave devices. Consequently, 60 GHz communication is unlikely to be a drop-in replacement for existing non-LOS (NLOS) WiFi and cellular networks in the near future.

While communication near 60 GHz likely has many future applications, given that it is unlikely to be a complete replacement of current wireless technologies, recent attention has focused on the upper microwave and lower mm-wave bands from 15-38 GHz that offer high bandwidth but may offer more favorable propagation conditions and lower device costs. Recent work has characterized indoor and outdoor propagation at 28 GHz [16–21] and 24 GHz [22–25]. As discussed in Section II, these studies show that path loss at these frequencies is similar to that at UHF frequencies in outdoor channels and is lower than that at 60 or 73 GHz in indoor NLOS environments.

The preliminary studies discussed above and more fully in Section II suggest that systems operating in the 15-38 GHz range may support high-throughput NLOS transmissions more readily than systems operating at 60 GHz. However, to date, only preliminary examination of the spatial multipath structure has been explored. Furthermore, there is limited exploration of the differences between propagation when the radios have omni-directional or directional antennas, with most measure-

This work was supported in part by the U. S. Army Research Office under Grant # W911NF-12-1-0469.

R. Mehmood is with Wavetronix, LLC, Provo, UT 84606, e-mail: r.mehmood@ieee.org.

J. Wallace, W. Ahmad, and Y. Yang are with Lafayette College, Easton, PA 18042, e-mail: wall@ieee.org, ahmadw@lafayette.edu, yangy@lafayette.edu.

M. Jensen is with Brigham Young University, Provo, UT, 84602, e-mail: jensen@byu.edu

[1]The FCC recently released 7 GHz of additional spectrum near 60 GHz, meaning 14 GHz for unlicensed use from 57-71 GHz (FCC-16-89).

ments inferring properties for omni-directional excitation from directional measurements.

The objective of this work is therefore to characterize path loss, delay spread, and MIMO performance in the 24 GHz band in indoor environments under both LOS and NLOS conditions when both types of antennas are used. The analysis is based on measurements performed with 4×4 channel sounders at both Brigham Young University (BYU) and Lafayette College (LC) [26, 27]. Ray-tracing simulations are also used to facilitate understanding of the observed channel characteristics. In order to assess the suitability of such a band to support systems that can replace current systems operating at lower frequencies, we compare the characteristics at 24 GHz to co-located measurements performed at 2.55 GHz. While preliminary measurements have been reported in prior publications [27, 28], these publications reported only limited results from the BYU campaign without the comparisons to LC measurements, measurements at 2.4 GHz, and ray-tracing.

II. Background

Before discussing the measurement campaigns and data analysis documented in this paper, it is useful to summarize key observations of past research on propagation characterization in the upper microwave and lower mm-wave bands.

Most recent work has focused on communication near 28 GHz as a suitable band for indoor and outdoor wireless communication. Perhaps the most extensive analysis of the outdoor environment provides comparative measurements at 28, 38, 60, and 73 GHz, with measurements performed using directional antennas that are steered in azimuth and elevation [16]. The work provides both directional and omni-directional path loss models, showing that the path loss increases as R^n with R representing the propagation distance and n assuming values in the range 1.8-2.1 in LOS environments and 2.4-3.5 in NLOS environments, ranges that are comparable to those observed for UHF communication. The findings suggest that in outdoor environments, path loss for propagation distances beyond 1 m is relatively insensitive to frequency. In contrast, this campaign revealed that the the root-mean-square (RMS) delay spread measured using directional antennas in the outdoor environment drops from 17.1 ns at 28 GHz to 11.4 ns at 38 GHz (which is comparable to the 11.1 ns delay spread observed at 73 GHz).

A similar measurement campaign used horn antennas to explore channel characteristics in an indoor environment at 28 and 73 GHz [17]. Results from this campaign confirm that for LOS communication, the co-polarized path loss exponent is only weakly dependent on the frequency and is slightly lower for omni-directional antennas ($n \approx 1.2$) than for directional antennas ($n \approx 1.7$). Additional frequency sensitivity is observed for NLOS communication, with path loss exponents of $n = 2.7$ ($n = 4.4$) and $n = 3.2$ ($n = 5.3$) at 28 and 73 GHz, respectively, for omni-directional (randomly oriented directional) antennas, a scale of frequency dependence not observed in NLOS outdoor channels [16]. Average co-polarized RMS delay spread values were found to be 17.3 ns (12.8 ns) and 17.7 ns (12.3 ns) for LOS and NLOS conditions, respectively, at 28 GHz (73 GHz) when averaged over all antenna directions. When antennas were pointed in the directions giving highest power, RMS delay spread dropped to 4.1 ns (3.6 ns) and 13.4 ns (11.3 ns) for LOS and NLOS at 28 GHz (73 GHz). Additional publications have captured the findings from these measurements in channel path loss models [17–19, 29]. Standardization of channel models for 5G communications in the 6 to 100 GHz range is currently under discussion. For example, channel modeling above 6 GHz is addressed by the overview in [30] as well as by 3GPP [31].

Recent measurements were also performed in downtown Daejeon, South Korea, at 28 and 38 GHz with omni-directional and horn antennas, both in an outdoor urban area and inside an airport terminal [20]. Scalar path loss and multipath parameters were extracted and compared with those from existing sub-6 GHz models. The results show that median path loss exponents ranged from $n = 2.0$ to 3.0 for the various LOS and NLOS environments. Median RMS delay spread in LOS (NLOS) at 28 GHz was 10.8 ns (44.6 ns) outdoors and 42.5 ns (108 ns) indoors, somewhat higher than the values reported in [17]. The study found remarkable similarity of extracted parameters at 28 and 38 GHz compared to those from sub-6 GHz models. Short-range propagation ($\approx$ 7 m) at 28 GHz was investigated in an indoor laboratory environment in [21] using a rotating directional antenna. Although some multipath was seen and used to develop a cluster-based model, RMS delay spread was only on the order of 4.5 ns.

Co-located measurements at 29 GHz and 2.9 GHz were performed in a Qualcomm office building in Bridgewater, NJ [32]. Measurements employed omni-directional antennas and spherical scanning directional antennas. Characterization of the data was simplified by defining *near* and *far* scenarios, where the transmit-receive separation was below or above 10 m, respectively. NLOS path loss exponents were $n = 2.2$ ($n = 4.9$) and $n = 2.6$ ($n = 5.2$) for the near (far) cases at 2.9 and 29 GHz, respectively. Median RMS delay spread was approximately 40 ns and 30 ns at 2.9 and 29 GHz, respectively. An exponential distribution provided a good fit to excess delay in both bands.

Because 24 GHz is relatively close to 28 GHz (from a fractional difference perspective), propagation conditions at these two frequencies are not expected to differ dramatically, aside from higher H_2O absorption at 24 GHz. Some limited work has provided additional understanding of radio characteristics at 24 GHz, with most focusing on the indoor environment [22–24, 33]. One notable study explored the relative path loss with reference to free space path loss (FSPL) at various frequencies between 2.4 GHz and 24 GHz using directional horn antennas. The study concludes that the excess path loss relative to FSPL is frequency independent in LOS conditions, but creates 10-20 dB of additional loss at 24 GHz compared to observations at 2.4 GHz in an NLOS hallway scenario [22]. Surprisingly, this study also finds mean RMS delay spreads in NLOS environments to be higher at 24 GHz ($\approx$ 52 ns) than at 2.45 GHz ($\approx$ 20 ns), a finding that is in contrast to results observed at 28 GHz.

Another study used highly directional antennas (3.5° beamwidth) to characterize the path loss at 24 GHz in an

indoor environment [23]. Experimental results revealed that in a curved corridor, the observed path loss is less than the FSPL (estimated $n = 1.4$ [24]), which the authors of the study attributed to a waveguiding effect. This work also provided results from a limited study on the attenuation of various building materials at 24 GHz.

In [33] indoor channels were measured with rotating directional antennas at 24 GHz and 5.3 GHz in a hallway environment and fit to the Saleh-Valenzuela model. Results indicate narrower angular spreads and (surprisingly) longer reverberation of 24 GHz signals than of 5.3 GHz signals. The work in [34] compared measured path loss characteristics at 24 GHz in urban and sub-urban scenarios using directional antennas. A proof-of-concept 24 GHz channel sounder based on optical signal generation was presented in [35].

III. Measurement Systems and Locations

Four prototype channel sounders were employed to perform the MIMO channel measurements used in this analysis. The LC 2.55 GHz and 24 GHz sounders as well as the BYU 2.55 GHz sounder use the architecture described in [26], employing discrete tones as the probing signal. The BYU 24 GHz sounder is fundamentally different, using a chirp probing signal. All sounders use switched arrays for MIMO measurements, with parameters summarized in Table I. These sounders, along with the measurement locations, are described here in detail.

A. 2.55 GHz

An important goal of this work is to compare MIMO propagation characteristics in the 24 GHz ISM band to those observed at 2.4 GHz. Given significant indoor interference at 2.4 GHz due to existing WiFi systems, measurements in the lower band were performed instead at 2.55 GHz, which was found to be very quiet at both BYU and LC.

The measurement systems used for 2.55 GHz measurements at BYU and LC are 8×8 switched MIMO channel sounders operationally equivalent to the one presented in [26]. Although the 2.55 GHz BYU system sends a multitone signal with 20 MHz bandwidth, the 2.55 GHz LC system uses only a single transmit frequency due to limitations of the signal source. The equipment for transmit and receive nodes is placed on carts that can be easily moved during the measurement.

In the BYU 2.55 GHz measurements, simultaneous directional patch and omni-directional monopole measurements were performed by subdividing each 8-element array into 4 patches and 4 monopoles, as shown in Fig. 1. The monopole antennas are assumed to be omni-directional. Simulations of the square patch used in these measurements indicate a peak antenna gain of 6 dBi, with 3 dB beamwidths (HPBW) of 80° and 176° in the horizontal (azimuth) and vertical (elevation) planes, respectively. In the LC 2.55 GHz measurements, only monopoles were used, but each 8-element array consisted of two 4-element arrays arranged in a cross, allowing two orthogonal array orientations to be probed with a single measurement.

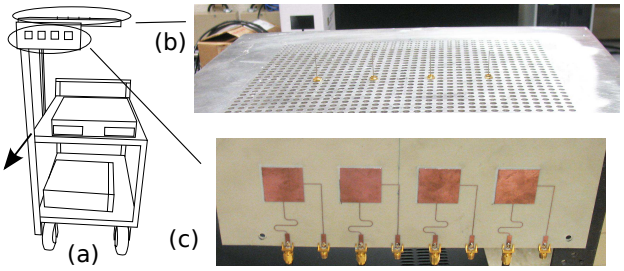

Fig. 1. Antenna array used for the 2.55 GHz BYU measurements: (a) Setup of the transmit cart showing location of arrays, (b) monopole array, (c) patch array. The arrow perpendicular to the patch array is the orientation direction referred to in later discussion.

B. 24 GHz

The new channel sounder hardwarewas developed at BYU and LC to support this research were based on the switched architecture. A schematic diagram of the BYU 24 GHz channel sounder is depicted in Fig. 2(a).

The local oscillator (LO) is a 12 GHz sweeper phase-locked loop (PLL) board, based on the Analog Devices ADF4159 device. The LO sweeps from 11.875 GHz up to 12.125 GHz in 1 ms and then back down in 1 ms. This chirp waveform is divided, where half of the power is frequency doubled (x2), attenuated as needed, and delivered to an RF-over-fiber (ROF) link. The ROF link consists of an optical transmitter (OT), 70 m of optical fiber (OF), and the optical receiver (OR). It was found that having more optical fiber than is needed for the measurement distance was useful to provide a frequency offset of approximately 200 kHz in the receiver, which avoids low-frequency interference at baseband. This delay-induced frequency offset is small enough to keep signals within the bandwidth of the A/D converter, thus requiring no special compensation in the receiver. The transmit subsystem power amplifies the 24 GHz chirp by 15 dB and delivers this signal to one of four transmit antennas using a SP4T switch. The signal from each switch port is power amplified by an additional 15 dB before being sent to the transmit array.

After propagating through the channel, the 24 GHz chirp signal is received by the array, where each branch is amplified with a low-noise amplifier (LNA) with 20 dB gain and a noise figure of 2.2 dB. The signal from one of the receive branches is fed to a common receiver chain using another SP4T switch. This signal is further low-noise amplified by 50 dB and mixed down to baseband using a sub-harmonic mixer pumped with the 12 GHz chirp LO. The baseband signal is low-pass filtered and sampled at 1 MS/s and 16-bit resolution using a National Instruments data acquisition board installed in a PC. MATLAB is used as the scripting language to automate acquisition and perform processing of the data. The complete 4×4 channel matrix is scanned in 40 ms in a multiplexed fashion, where synchronization (SYNC) units provide digital control to the SP4T switches, and each SYNC is driven with a Rubidium (Rb) 10 MHz reference.

Given the large dynamic range required for 24 GHz channels along indoor routes, fixed attenuators can be added and one level of PA removed to reduce transmit power. Gain of the attenuators and the swappable PA were carefully measured

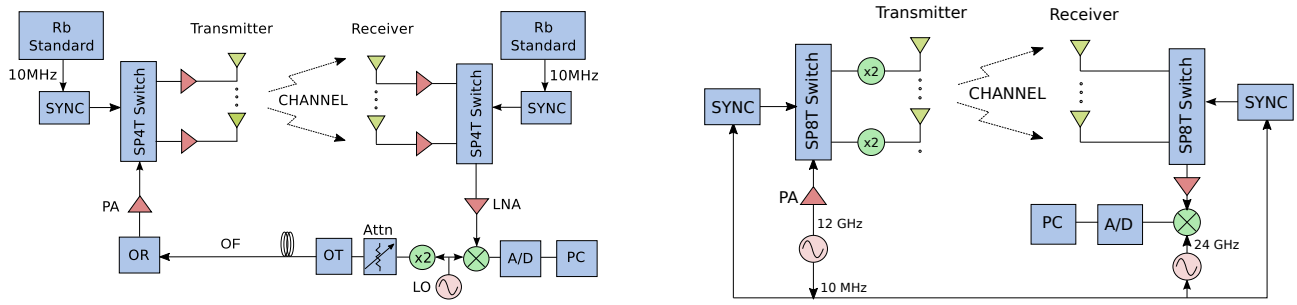

(a) BYU (b) LC

Fig. 2. Block diagrams of the 24 GHz measurement systems used at (a) BYU and (b) LC.

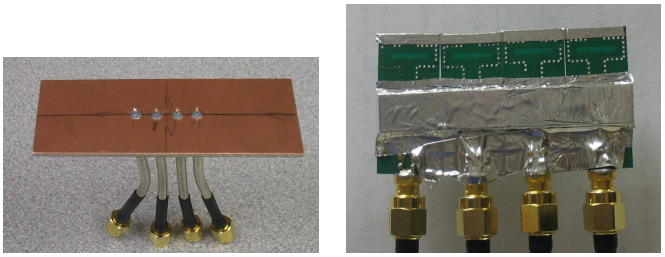

(a) Monopoles (b) Slot Antennas

Fig. 3. Antenna arrays used for the 24 GHz BYU and LC measurements: (a) Monopole array with $\lambda/2$ spacing, (b) vertically polarized slot array with 1.2λ spacing.

TABLE I
CHANNEL SOUNDER PARAMETERS

	24 GHz		2.55 GHz	
	BYU	LC	BYU	LC
Probe Signal	Chirp	CW	4 Tones	CW
Bandwidth	500 MHz	-	20 MHz	-
Tx Power	20 dBm	13 dBm	23 dBm	23 dBm
LNA	70 dB	45 dB	40 dB	40 dB
Synchronization	Optical	Cable	Rubidium	Cable
Antenna Types	Monopole, Slot	Monopole	Monopole, Patch	Monopole
Slot/Patch Gain	5 dBi	N/A	6 dBi	N/A
HPBW	75°/150°	N/A	80°/176°	N/A
Arrays	4×4 ULA	4×4 ULA	8×8 ULA	8×8 ULA
Snapshot Time	40 ms	0.84 ms	3.0 ms	3.0 ms
Freq. Bins N_F	1000	1	4	1
Max. Link Loss	145 dB	130 dB	135 dB	140 dB

with a VNA, allowing the correct transmit power to be properly accounted for in processing. The repeatability of results when changing these components is better than ± 0.5 dB.

A block diagram of the LC 24 GHz sounder is shown in Fig. 2(b). This system only transmits a single tone to investigate channel path loss and multipath characteristics. To this end, a microwave source at the transmitter generates a 12 GHz tone that is power amplified and fed to a SP8T switch. The signal from each switch output port is fed to an active frequency doubler that also provides amplification, resulting in a 24 GHz transmit tone at 13 dBm. At the receive side, the signal from one antenna at a time is fed to the common receiver chain using a SP8T switch. The common signal is low-noise amplified by 45 dB, mixed down to a 50 MHz intermediate frequency (IF), sampled using 100 MS/s 12-bit analog-to-digital (A/D) conversion, and stored on a PC. Antenna and switch synchronization is achieved using a common 10 MHz reference supplied by the transmit microwave source to the receiver using a long coaxial cable. This single-tone system scans the complete channel in 0.84 ms. Note that although up to 8 antennas can be supported at transmit and receive, only 4 antennas were used with each array in this study.

The antennas that were used at 24 GHz with both the BYU and LC systems are quarter-wave monopoles with $\lambda/2$ inter-element spacing and directional vertically-polarized slot antennas with 1.2λ inter-element spacing, depicted in Fig. 3(a) and (b), respectively. The monopole antennas are assumed to be omni-directional. The slot antennas have a ground plane backing creating a uni-directional beam, where simulations indicate a peak gain of 5 dBi with 3 dB beamdwidths of 75° and 150° in the horizontal (azimuth) and vertical (elevation) planes, respectively.

C. Data Processing and Calibration

The 2.55 GHz BYU system and both the 2.55 and 24 GHz LC systems are based on sending discrete tones, and processing and calibration methods for this signal can be found in [26]. The 24 GHz BYU system requires some additional explanation. As described in the hardware section, the received signal is mixed down with the same chirp used for transmit, similar to a frequency-modulated continuous-wave (FMCW) radar. Taking a fast-Fourier transform (FFT) of the resulting baseband signal yields the complex impulse response (CIR) of the channel. Only the 1 ms up-chirps are processed, where each 1000-sample chirp is Blackman windowed before applying the FFT.

The power-delay profile (PDP) is obtained by averaging the magnitude squared of the CIR over all pairs of antennas and over 100 temporal snapshots. The noise floor is clearly visible in each PDP plot and is found automatically in processing using the 50% level of the PDP cumulative distribution function (CDF), where the *signal threshold* is assumed to be 3 dB above that noise floor. The data is de-noised by zeroing CIR and PDP delay bins with power below the signal threshold. Baseband interference is removed by zeroing bins that have a delay less than half of the minimum possible system delay. Link gain and RMS delay spread are computed from the PDPs, meaning that

TABLE II
BYU-CB ARRAY ORIENTATIONS

Set	Orientation	
	Transmit	Receive
TA-R1	→ (E)	Along Route
TA-R2	← (W)	Along Route
TA-413 W,S	→ (E)	← (W), ↓ (S)
TA-406 E,S	← (W)	→ (E), ↓ (S)
TA-425 E,N	← (W)	→ (E), ↑ (N)
TA-400 E,S	← (W)	→ (E), ↓ (S)
TA-490 E,S	← (W)	→ (E), ↓ (S)
TB-R3 A,O	→ (E), ← (W)	Along (A), Opposite (O) Route

all delay bins with power above the signal threshold contribute to these computations.

Frequency-domain channel responses are obtained by performing an additional FFT on the de-noised CIR. Note that non-averaged CIRs are used for capacity computations since averaging may alter the spatial structure of the MIMO channels. The system is calibrated by successively connecting each transmit port to each receive port and storing the amplitude and phase associated with the first peak of the CIR. These calibration coefficients are then used to normalize the data, which calibrates measurements up to the antenna ports. Since the antenna gains are not removed from measurements, link gain plots include antenna gain effects, allowing easy visualization of system link budgets.

D. Measurement Campaign

It is well established that lower microwave frequencies, such as those in the 2.4 GHz ISM band, are well suited for NLOS communications in an indoor environment. One important goal of this study is to determine what level of obstruction can be tolerated for NLOS communications in the presence of higher attenuation at 24 GHz.

In measurements at both BYU and LC, the transmitter was usually placed in a central hallway, while the receiver was placed in connecting hallways or rooms. The idea is to simulate a common method of WiFi coverage, where access points are placed at key points on main hallways, thus serving users in connecting hallways or rooms. To avoid confusion, note that each transmit position is labeled with T followed by a letter (TA, TB, etc.). Receive positions are labeled with R followed by a number (R1, R2, etc.) for hallway routes or by the room number (without R) for stationary room measurements. The label "Rooms" (or RM for short) is used to refer to all room receive positions collectively. Data sets names are coded using transmit-receive label pairs like TA-R1, TB-425, or TC-Rooms. *Route distance* refers to distance traveled along a measurement route from a starting position, i.e. the Manhattan grid distance, whereas *path distance* refers to the actual Euclidean distance between transmit and receive. For route-based measurements, the receiver was not moved continuously but rather in discrete steps between measurements.

1) BYU: Measurements were taken on the 4th and 5th floors of the Clyde Building (CB) as depicted in Fig. 4. For the 4th floor measurements (BYU-CB4), the transmitter was placed at location TA in a central corridor and the receiver was moved along paths R1 and R2. Stationary receiver room

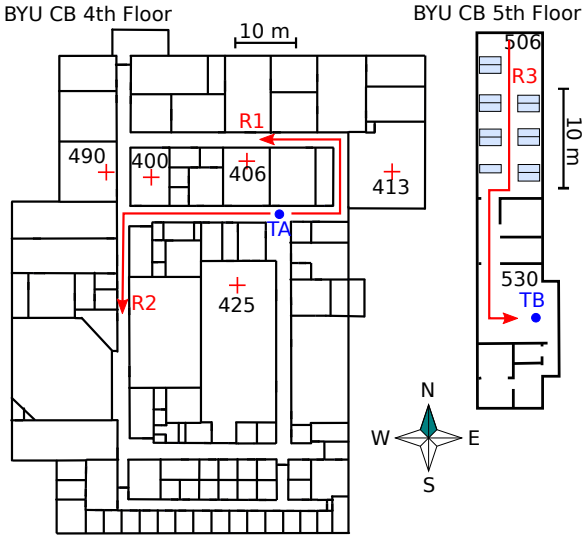

Fig. 4. Measurement locations on the 4th (left) and 5th (right) floors of the Clyde Building on the BYU campus. TA and TB represent fixed transmitter locations, while R1-R3 are receiver routes. Fixed measurement points in rooms are indicated by plus symbols (+). Large metal work benches in Room 506 are also depicted.

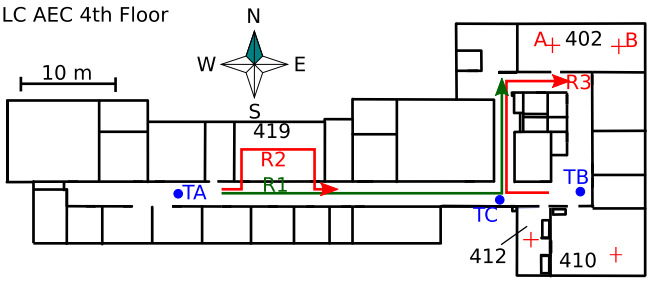

Fig. 5. Measurement locations on the 4th floor of the Acopian Engineering Center (AEC) at LC. TA-TC represent fixed transmitter locations, while R1-R3 are receiver routes. Fixed receive measurement points in rooms are indicated by plus symbols (+).

measurements were also taken at the locations marked by '+'. Since directional patches were used, the orientation of the arrays was important. Table II summarizes the orientations that were used for each of the sets. The term *along (or opposite) route* for TA-R1 and TA-R2 indicates that the receive antenna arrays faced in (or opposite) the direction of the route arrow in Fig. 4, which changes during the route. Labels like TA-413 W,S refer to two separate data sets (TA-413W and TA-413S) where the receiver is pointed west and south, respectively. Also, TB-R3 A,O indicates two separate route measurements with the receiver antenna pointed along or opposite the route. Note that the goal in the BYU-CB4 measurements was generally to point the Tx and Rx patch arrays toward each other. The one exception is the 5th floor measurements (BYU-CB5), where one case investigated directional antennas pointing away from each other.

2) Lafayette College: Measurements at LC were taken on the 4th floor of the Acopian Engineering Center (AEC) as depicted in Fig. 5. Measured Tx-Rx pairs and orientations of arrays for the LC-AEC data are listed in Table III, using the same nomenclature as that for BYU-CB.

TABLE III
LC-AEC ARRAY ORIENTATIONS

Set	Orientation Transmit	Receive
TA-R1	→ (E),↑ (N)	Along Route
TA-R2	→ (E),↑ (N)	Along Route
TB-R3	← (W),↑ (N)	Along Route
TC-402 N,E	↑ (N)	↑ (N), → (E)
TC-410 N,E	↑ (N)	↑ (N), → (E)
TC-412 N,E	↑ (N)	↑ (N), → (E)
TC-419 N,E	↑ (N)	↑ (N), → (E)

IV. RAY-TRACING SIMULATIONS

Due to the difficult and time-consuming nature of measurements, we also investigate whether ray-tracing (RT) simulations can provide the same information more conveniently. The BYU-CB4 and LC-AEC4 indoor environments were modeled with the Wireless InSite tool from Remcom. The tool returns path parameters (directions of arrival and departure, delays, and gains) in a text file for each simulation point, allowing coherent MIMO channels to be computed in MATLAB. Floor plans for the two scenarios were created using the tool, which included walls, doors, floor, and ceiling. Furniture was only included in one of the simulated cases in order to try to improve the fit, as explained later. Initially, stock material parameters built into the tool were used, but these were later changed to try to improve the fit of simulations and data. Overall, we found that material loss (conductivity) had to be increased, especially at 24 GHz, to reach an acceptable fit.

Using a constant number of rays in all scenarios did not provide a good fit to the measurements. For example, at 24 GHz with higher loss, an increase in reflected rays was often needed to connect transmit to receive, whereas at 2.55 GHz, rays penetrating through walls were more common, thus requiring fewer rays. The number of transmitted rays at 24 GHz was initially set to the relatively high values used at 2.55 GHz, but where necessary we reduced transmitted rays in favor of more reflected rays while maintaining a similar run time. Although the RT tool supports a surface roughness parameter for materials, we found negligible change in simulated results using this feature. The need to change material parameters and the number of rays reveals the importance of correct material parameters as an input to ray-tracing studies in the near mm-wave bands. Since such parameters are not readily available, future work is needed to carefully characterize materials between the microwave and mm-wave bands.

Table IV summarizes the measurement cases that were simulated in Wireless InSite, along with the material parameters and number of ray orders. In the table, RM refers to all room receive locations, ϵ_r is the relative permittivity, σ is the conductivity, and Δ is the thickness. In the AEC, interior walls were simulated as a stack of drywall/air/drywall, and therefore the material parameters are listed as triplets in the table. To improve the fit to the data, walls on the perimeter of the AEC floor plan in Fig. 5 were modeled as *exterior* "E:" walls made of reinforced concrete, while those inside the floor plan were modeled as *interior* "I:" walls made of drywall. It is likely that some interior walls are also concrete, but these details were not available when capturing the building model in this study. The maximum order or level of reflection, transmission, and diffraction used in the RT tool is listed as the R/T/D triplet. In all cases the floor and ceiling material were concrete, with $\epsilon_r = 15$, $\sigma = 0.015$ S/m, and thickness 30 cm.

TABLE IV
RAY-TRACING SIMULATION PARAMETERS

2.55 GHz BYU-CB							
	Wall Material			Door Material			Order
		S/m	cm		S/m	cm	
Set	ϵ_r	σ	Δ	ϵ_r	σ	Δ	R/T/D
TA-R1	5	0.05	15	2	0.05	5	6/6/0
TA-R2	5	0.01	15	2	0.01	5	8/6/0
TA-RM	5	0.01	15	2	0.01	5	8/4/1
24 GHz BYU-CB							
Set	ϵ_r	σ	Δ	ϵ_r	σ	Δ	R/T/D
TA-R1	10	0.5	10	10	0.5	5	12/2/0
TA-R2	5	0.01	10	5	0.01	5	6/6/0
TA-RM	10	0.3	10	5	0.3	5	15/4/0
2.55 GHz LC-AEC							
Set	ϵ_r	σ	Δ	ϵ_r	σ	Δ	R/T/D
TA-R1	5/1/5	0.1/0/0.1	2/9/2	5	0	3	6/6/0
TA-R2	5/1/5	0.1/0/0.1	2/9/2	5	0	5	12/4/0
TB-R3	5/1/5	0.1/0/0.1	2/9/2	5	0	5	6/6/0
TC-RM	I:5/1/5	I:0.1/0/0.1	I:2/9/2	5	0	5	15/2/1
	E:15	E:5	E:25				
24 GHz LC-AEC							
Set	ϵ_r	σ	Δ	ϵ_r	σ	Δ	R/T/D
TA-R1	10/1/10	0.3/0/0.3	2/9/2	5	0.3	5	12/4/0
TA-R2	10/1/10	0.3/0/0.5	2/9/2	5	0.3	5	12/4/0
TB-R3	10/1/10	0.3/0/0.3	2/9/2	5	0.3	5	12/4/0
TC-RM	I:10/1/10	I:0.1/0/0.1	I:2/9/2	5	0.1	5	15/2/1
	E:15	E:5	E:25				

V. CHANNEL CHARACTERIZATION

A. Power Delay Profiles

Fidelity of the data in the new 24 GHz FMCW system was first verified by plotting PDPs for the measured channels. Fig. 6 shows example raw (not de-noised) PDPs for the start and end of the route for BYU-CB5 TB-R3 with monopoles, aligned slots, and opposite-facing slots. As can be seen, the instantaneous dynamic range of the system is about 40 dB. The overall dynamic range is much higher, since amplifiers and attenuators can be removed during the measurement. The raw PDP also shows significant interference at lower delays, corresponding to low-frequency interference in the baseband signal. These spurious signals are due to low-delay Tx-Rx feed through and interference from various sources. A benefit of the ROF system is the ability to place additional delay and move our signal of interest well past any of this low-frequency interference. Due to space constraints, other PDPs will not be shown, but the key information can be obtained from the RMS delay spread metric analyzed in Section V-C.

B. Link Gain and Path Loss

Link gain estimates are obtained by averaging the received channel power over all Tx-Rx antenna pairs at a location as well as over frequencies and snapshots (if applicable). Channel power for wideband 24 GHz BYU measurements was obtained by integrating de-noised PDPs in linear power. The plots provide the link gain (negative of link loss in dB).

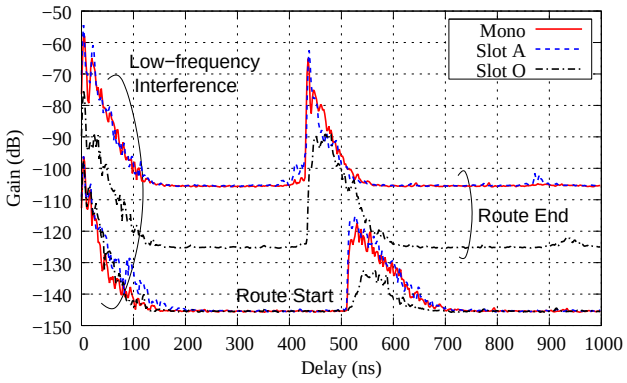

Fig. 6. Raw (not de-noised) power-delay-profile averaged over all antennas and snapshots for the start and end of the route of data set BYU-CB5 TB-R3. Curves are for monopoles (Mono), aligned slots (Slot A), and opposite-facing slots (Slot O).

According to the Friis transmission equation, received power varies according to $20\log_{10}\lambda$ [dB], where λ is the wavelength and all other parameters are held constant. Given identical antenna gains at 2.55 and 24 GHz, a 10-fold increase in frequency leads to a 20 dB reduction in receive power. We refer to this as *aperture loss*, since it is due to a smaller receive antenna aperture for constant gain. Boosting the 24 GHz curves by 20 dB provides insight into how much *excess loss* above the aperture loss is present. We define excess loss as $L_{\text{excess}}(d) = G(f_0, d) - [G(f_1, d) + 20\log_{10}(f_1/f_0)]$ where $G(f, d)$ is a link gain measurement in dB at frequency f and position d, and f_0 and f_1 are 2.55 and 24 GHz, respectively. The comparison is reasonable since quarter-wave monopoles are expected to behave similarly at the two frequencies, and simulations show that the directional antennas are also similar in terms of gain and beamwidth.

1) BYU-CB4: The link gain versus route distance for BYU-CB 4th floor locations (TA-R1, TA-R2, and TA-Rooms) is shown in Fig. 7. As expected, the link loss is much higher at 24 GHz than at 2.55 GHz. In the hallway under LOS or around a single corner, there is very little difference in the loss at the two frequencies when including the 20 dB compensation. The RT simulations compare favorably to the measured results, with the main exception being that power for TA-Rooms at 2.55 GHz is over-predicted by 5-15 dB. Since material parameters were only slightly tuned at 2.55 GHz, we expect RT is over-predicting penetration through the cinder block walls. The results show that the fit for TA-R2 is quite good.

2) LC-AEC4: Link gain versus distance for three LC-AEC locations (TA-R2, TB-R3, and TC-Rooms) is shown in Fig. 8. As shown, the 20 dB aperture compensation only provides a good fit between 2.55 GHz and 24 GHz for the hallway LOS positions. RT simulations fit well to the data in some cases, but not others, indicating the difficulty of fitting the propagation data with a single hand-tuned set of material parameters. In particular, the set TC-Rooms was difficult to fit with RT, likely due to the highly obstructed nature of the channel. It was necessary to include some metal shelves and cabinets to block the direct though-wall path to Room 410 to improve the fit.

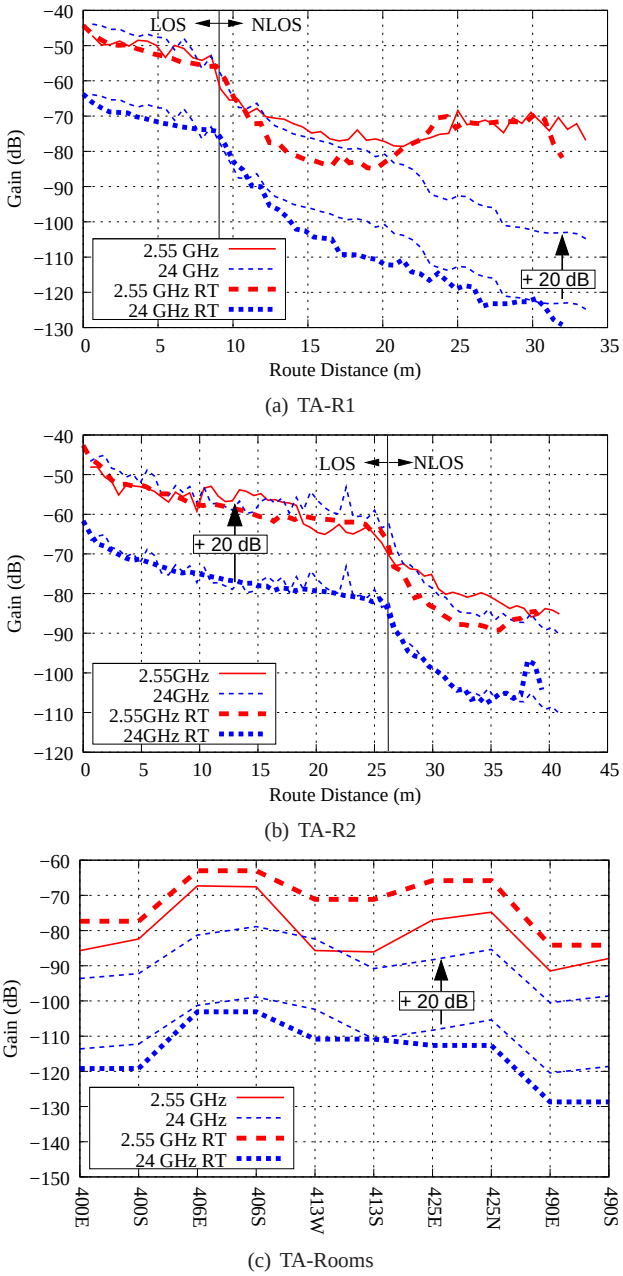

(a) TA-R1

(b) TA-R2

(c) TA-Rooms

Fig. 7. Link gain for CB4 measured data compared with RT simulations. For the 24 GHz measured data, the actual data (lower curve) is boosted by +20 dB to obtain the upper curve, showing the effect of aperture loss compensation.

Comparing Fig. 8 with Fig. 7 shows that loss in the AEC is somewhat higher than that observed in the CB.

Fig. 9 plots CDFs of gain for all BYU-CB-TA data, all LC-AEC data, and all RT simulations. The plot confirms that the loss in the CB at 24 GHz is less than that observed in the AEC. More importantly, however, the difference between the 2.55 and 24 GHz curves is approximately 30 dB at the 50% level. The results also show that RT provides a reasonable prediction of the link loss distribution at both frequencies.

3) BYU-CB5: Next we consider link loss using measurements from data set BYU-CB5, where both monopole and directional slots or patches were used. Fig. 10(a) shows link gain as a function of route distance when the directional

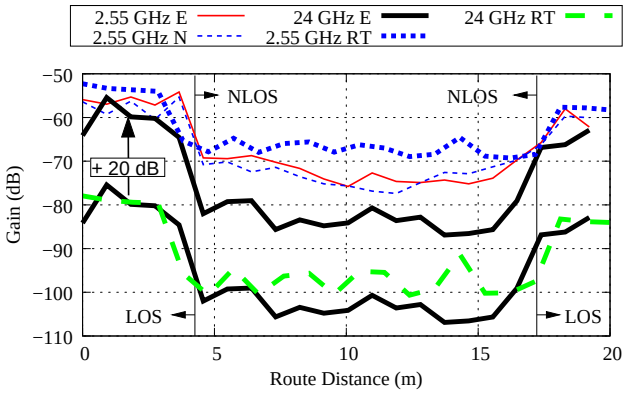

(a) TA-R2

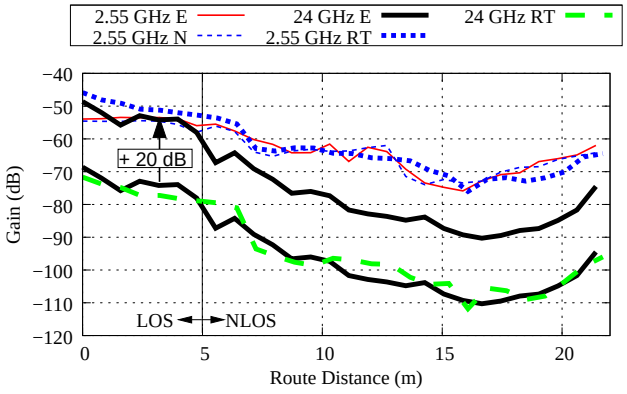

(b) TB-R3

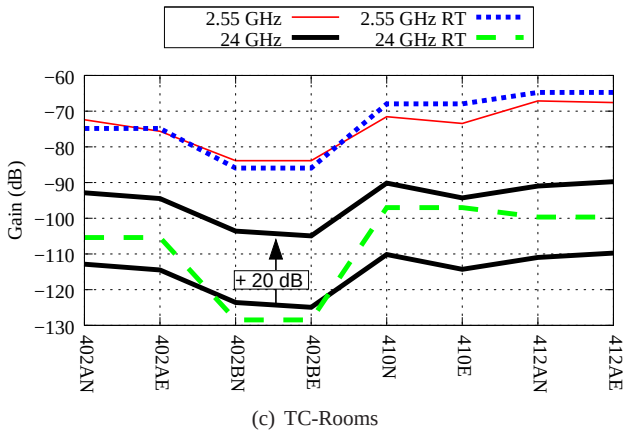

(c) TC-Rooms

Fig. 8. Link gain for AEC4 measured data compared with RT simulations. For the (a) TA-R2 and (b) TB-R3 data, two different transmit orientations (E,N) were considered, while for (c) TC-Rooms data, two different receive orientations (E,N) were considered.

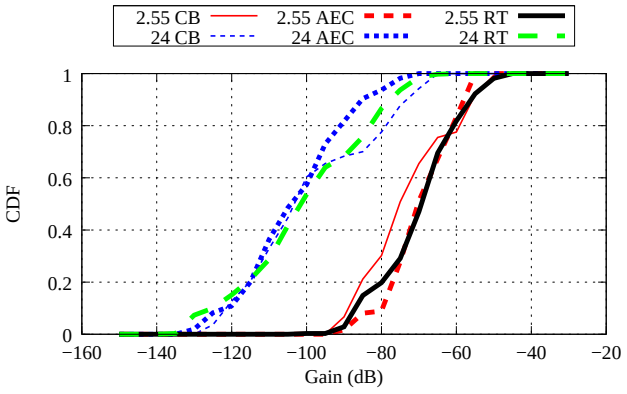

Fig. 9. Link gain CDFs for all data from BYU-CB-TA, LC-AEC, and RT.

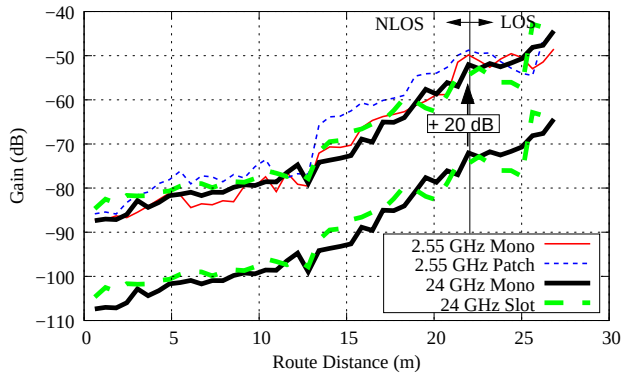

(a) TB-R3-A (Aligned)

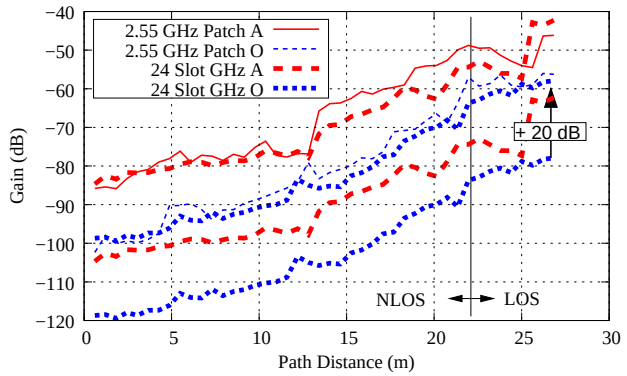

(b) TB-R3-O (Opposite)

Fig. 10. Link gain for CB5 measured data: (a) aligned directional antennas (patch, slot) compared to omnidirectional monopoles, (b) aligned directional antennas compared to opposite-facing directional antennas. Aperture compensated 24 GHz data (+20 dB) is also plotted.

Tx and Rx antennas are oriented along the route roughly toward one another (TB-R3 A). The plot indicates that the directional antennas provide 5-8 dB improvement at 2.55 GHz and only 1-5 dB improvement at 24 GHz. Good agreement between the 2.55 and 24 GHz measurements is obtained when compensating for the aperture loss (+20 dB boost). Fig. 10(b) shows the effect of array misalignment when the directional antennas point in opposite directions relative to the route. The mean (standard deviation) of the additional loss due to misalignment computed from this data is 12.7 dB ($\sigma = 4.2$ dB) at 2.55 GHz and 12.8 dB ($\sigma = 3.8$ dB) at 24 GHz, showing remarkable similarity in the two bands. These results show the potential for adaptive beamforming and/or antenna selection algorithms to improve performance in both bands.

4) Path Loss Comparison: Table V compares the excess loss metric at 24 GHz vs. 2.55 GHz for AEC and CB data. Excess loss for LOS is nearly zero and not tabulated. The laboratory room environment of CB5 appears to differ from the other scenarios, only experiencing 1.4 dB excess loss averaged over the three antenna types. Excess loss in LC-AEC is somewhat higher (14 dB) than in BYU-CB4 (9 dB). A weighted average of all data according to the number of data

TABLE V
NLOS EXCESS LOSS OF 24 GHz VS. 2.55 GHz

BYU	Sets	Mean	Std. Dev.	Weight
Hall-Hall	TA-R1, TA-R2	9.3 dB	11.4 dB	2
Hall-Rooms	TA-Rooms	8.6 dB	4.8 dB	1
Labs	TB-R3 (Monopole)	-0.2 dB	2.1 dB	1/3
	TB-R3 (Slots A)	2.4 dB	2.9 dB	1/3
	TB-R3 (Slots O)	1.9 dB	2.3 dB	1/3
LC	Sets	Mean	Std. Dev	Weight
Hall-Hall	TA-R1, TB-R3	14.8 dB	4.3 dB	2
Hall-Rooms	TA-R2, TC-Rooms	13.1 dB	5.4 dB	2
Average		10.6 dB	6.9 dB	

TABLE VI
EXTRACTED PATH LOSS EXPONENTS

	LOS		NLOS	
	2.55 GHz	24 GHz	2.55 GHz	24 GHz
BYU-CB	1.06	1.56	3.24	4.50
LC-AEC	0.61	2.19	1.98	4.16

sets per entry gives approximately 11 dB of average excess loss.

Figs. 11 and 12 plot all monopole path loss (PL) data from BYU and LC, respectively, separated into LOS and NLOS cases, computed as

$$\mathrm{PL}(f,d)\ [\mathrm{dB}] = G_T + G_R - G(f,d), \tag{1}$$

where $G(f,d)$ is the link gain at frequency f and distance d, and G_T and G_R are the transmit and receive antenna gains (assumed to be 5 dBi for quarter-wave monopoles). Also shown is the best fit to the mean close-in (CI) path-loss model [16]

$$\mathrm{PL}^{\mathrm{CI}}(f,d)\ [\mathrm{dB}] = \mathrm{FSPL}(f,d_0) + 10n\log_{10}\left(\frac{d}{d_0}\right), \tag{2}$$

where the reference free-space path-loss is $\mathrm{FSPL}(f,d_0) = G_T + G_R - G(f,d_0)$ and we chose $d_0 = 2.5$ m. The estimated path-loss exponent (PLE) n is found by computing $G(f,d_0) - G(f,d)$ and MMSE fitting to $10n\log_{10}(d/d_0)$. Extracted path-loss exponents are given in Table VI.

Although model predictions with the CI model are good for LOS data, deviations occur for NLOS data, especially at 24 GHz. This reveals the difficulty of applying path-loss models based on Euclidean distance to the hallway environment, where waveguiding effects may exist. When traveling around a corner, Euclidean distance may decrease whereas distance traveled by the guided wave increases. Power can also be higher than expected at larger distances as the receiver enters a new hallway and receives power from other hallway paths.

The accuracy of site-specific ray-tracing as depicted in Figs. 7 and 8 is quantified using root mean-squared error (RMSE) in Table VII, indicating better accuracy in hallway scenarios than propagation into rooms. CDFs of all BYU and LC gain data in Fig. 9 were compared with RT at the 50% level, where the difference is listed as "50% CDF" in Table VII.

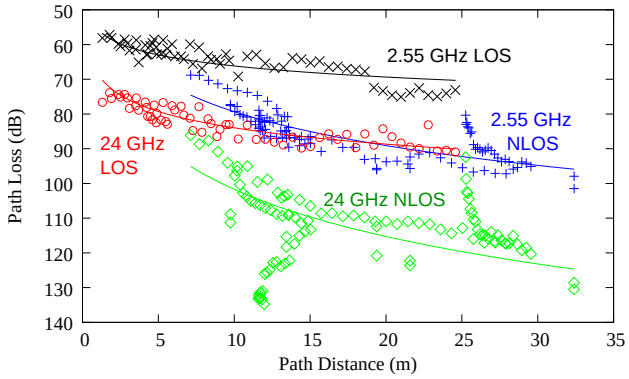

Fig. 11. Path loss versus path distance for all BYU-CB monopole data, with solid lines showing the best fit CI model.

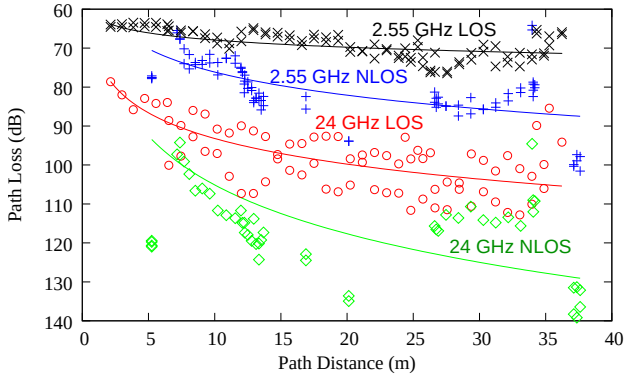

Fig. 12. Path loss versus path distance for all LC-AEC monopole data, with solid lines showing the best fit CI model.

C. RMS Delay Spread

As only the BYU 24 GHz system is able to provide PDP results, RMS delay spreads are only reported for these measurements. Fig. 13 shows the RMS delay spread of BYU-CB5 TB-R3 versus route distance. The monopoles and aligned slots give similar RMS delay spread, whereas the opposite-facing slots can give up to twice the delay spread, likely due to the removal of strong dominant paths.

Fig. 14 plots CDFs for each data set taken in the BYU-CB. Monopoles and aligned slots on the 5th floor provide the lowest delay spread, while opposite-facing slots on the 5th floor and monopoles on the 4th floor give similar delay spread. The longest delay spread was obtained for TA-Rooms, which also has the most attenuation due to obstacles.

Overall, the plots indicate that RMS delay spread in this indoor environment ranges from 10 to 50 ns, with median values ranging between 20 to 35 ns. These median values are similar to those of indoor 28 GHz channels reported in [17] (17 ns) and [20] (42.5 ns for LOS). The 28 GHz indoor laboratory channel in [21] exhibited a much smaller spread of 4.5 ns, likely due to the close transmit-receive separation. The peak delay spread of 50 ns is smaller than peak values observed near 2.4 GHz reported elsewhere [36], which often range from 50 to 150 ns. This can be understood by observing that the 24 GHz channels appear to exhibit only a single exponential cluster in delay, with the shape in Fig. 6 being

TABLE VII
RMSE OF RAY-TRACING VS. MEASUREMENT

BYU-CB	2.55 GHz	24 GHz
TA-R1	4.4 dB	5.0 dB
TA-R2	3.9 dB	2.6 dB
TA-Rooms	9.2 dB	6.4 dB
50% CDF	5.9 dB	1.8 dB
LC-AEC	2.55 GHz	24 GHz
TA-R2	5.7 dB	5.9 dB
TB-R3	3.6 dB	4.8 dB
TC-Rooms	3.0 dB	10.5 dB
50% CDF	0.9 dB	2.6 dB

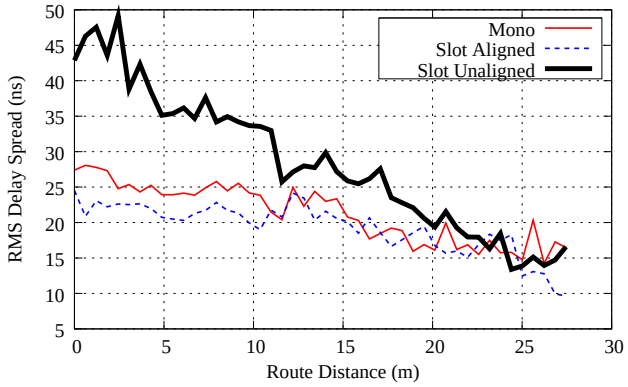

Fig. 13. RMS delay spread versus route distance for BYU-CB4 TB-R3 with various antenna types.

very typical. Unlike the 2.55 GHz band where high obstruction and rich scattering tend to produce multiple clusters, such obstructions only appear to make the single cluster somewhat wider at 24 GHz. Despite these differences, the median delay spreads observed at 24 GHz are very similar to the median values observed at 2.4 GHz in prior work [36].

D. Capacity

An important question is whether indoor channels support sufficient multipath richness in the 24 GHz band for MIMO communications, similar to what has been established in lower microwave bands. To explore this issue, we compute the maximal theoretical spectral efficiency (referred to simply as capacity for brevity) assuming an uninformed transmitter, computed as

$$C = \frac{1}{N_{\mathrm{F}}} \sum_{n=1}^{N_{\mathrm{F}}} \log_2 \left| \mathbf{I} + \frac{\rho}{N_{\mathrm{T}}} \mathbf{H}^{(n)} \mathbf{H}^{(n)H} \right|, \qquad (3)$$

where N_{F} is the number of frequency samples (listed in Table I), $N_{\mathrm{T}} = 4$ is the number of transmitters, $\mathbf{H}^{(n)}$ is the normalized channel matrix measured at the nth frequency sample, $\rho = 15$ dB is the assumed SNR, and $|\cdot|$ is the determinant. The choice of ρ is a critical issue when comparing capacity at 24 GHz and 2.55 GHz, and a proper choice depends on several factors: the relative level of noise and interference, system constraints and network topologies, the use of power control, etc. Since the primary goal of this section is to understand the presence of multipath for MIMO communications, we assume a constant SNR of 15 dB in all cases. Therefore, channel

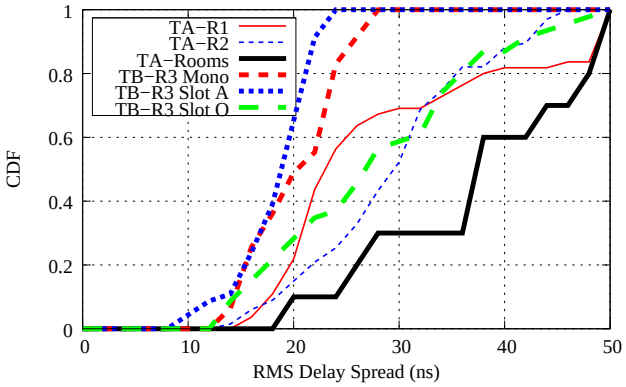

Fig. 14. CDFs of RMS delay spread for 24 GHz data sets taken in the BYU-CB.

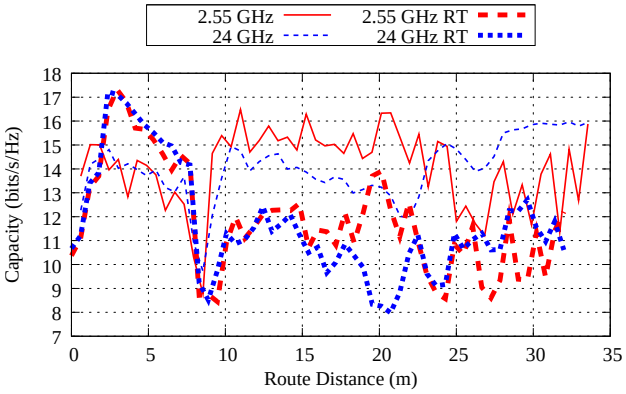

(a) BYU-CB TA-R1

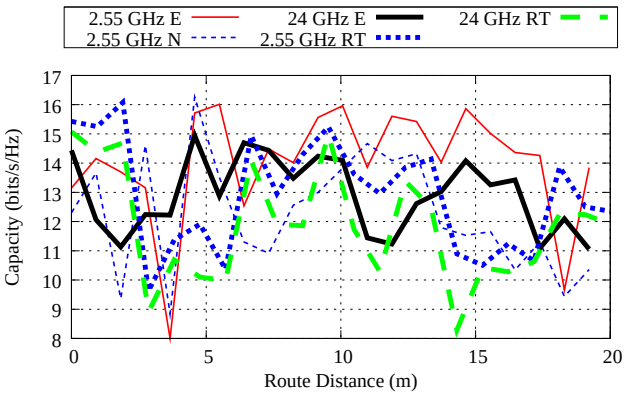

(b) LC-AEC TA-R2

Fig. 15. Site-specific capacity for two locations.

matrices were individually normalized for unit average single-input single-output (SISO) gain before computing (3).

Fig. 15 plots the capacity for (a) the hallway location BYU-CB TA-R1 and (b) the hallway and room location LC-AEC TA-R2. Although there are obvious differences in the 2.55 and 24 GHz measured data point-by-point, the trends are remarkably similar. The RT simulations provide a reasonable prediction up to the first turn in the receiver routes (9 m for (a) and 4 m for (b)). But we observe overall that the RT tends to under-predict capacity, a phenomenon that could be caused by not modeling furniture or diffuse scattering effects that increase multipath richness.

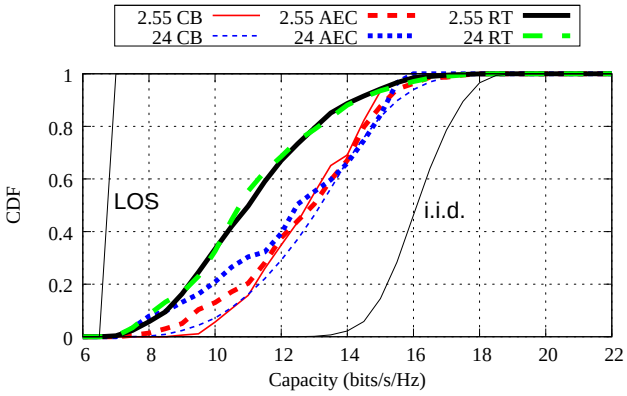

Fig. 16. Capacity CDFs comparing all data from BYU-CB4, LC-AEC, and RT. Capacity CDFs for simulated single-path (LOS) and i.i.d. channels are also shown for comparison.

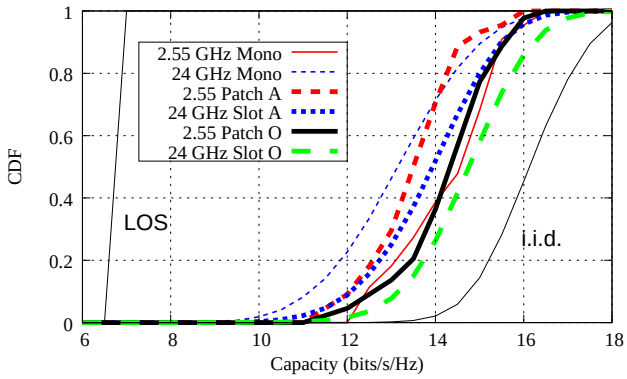

Fig. 17. Capacity CDFs comparing omni-directional antennas, aligned (A) directional antennas, and opposite (O) facing directional antennas for sets BYU-CB5 TB-R3 A,O. Simulated CDFs for single-path (LOS) and i.i.d. channels are also plotted.

Fig. 16 plots CDFs of capacity for all CB data, all AEC data, and all RT simulations. At the 50% probability level, there is very little difference between 2.55 GHz and 24 GHz capacity, and also little difference between the CB and AEC data. At a low outage level of 10%, we see that the CB has nearly identical capacity at 2.55 and 24 GHz (10 bits/s/Hz), while the AEC capacity is 9 bits/s/Hz at 2.55 GHz, and 8 bits/s/Hz at 24 GHz. This result emphasizes the remarkable similarity in spatial properties, at least in a statistical sense, at 2.55 and 24 GHz in the two indoor environments that were studied. This suggests that even though a single temporal cluster is seen at 24 GHz, paths within the cluster are sufficiently separated in angle, which was also observed in [37].

The effect of directional antennas and their alignment on capacity is shown in Fig. 17, which plots CDFs of capacity for data sets BYU-CB5 TB-R3-A and TB-R3-O. We first observe that all the antenna types give similar capacity that is much higher than that obtained in a simulated single-path (LOS) channel. At 2.55 GHz, aligned directional patches give lower performance than monopoles, likely due to reduced multipath richness caused by the narrower patch patterns. In contrast, the results for opposite facing patches that do not see the LOS component are similar to those for the monopoles at 2.55 GHz. The 24 GHz channel apparently exhibits reduced multipath, since the capacity achieved with monopoles at 24 GHz is lower than that obtained at 2.55 GHz. The improved performance of the 24 GHz aligned slots relative to the 24 GHz monopoles is likely due to the larger aperture given by the slot array (1.2λ versus $\lambda/2$ inter-element spacing). Finally, misaligned slots at 24 GHz had the highest capacity, indicating more multipath richness, but this comes at the expense of an average of 12.8 dB of additional link loss as seen previously. Such misalignment is unlikely to be useful with realistic link budgets and interference avoidance.

TABLE VIII
MEDIAN EDOF OF BYU AND LC DATA

	LOS		NLOS	
	2.55 GHz	24 GHz	2.55 GHz	24 GHz
BYU-CB	2.62	2.57	3.01	2.82
LC-AEC	2.37	2.15	2.95	2.97

Effective degrees of freedom (EDOF) [38] can also be used to quantify the potential for spatial multiplexing, computed as $\text{EDOF} = \sum_k [1 + N_T/(\sigma_k^2 \rho)]^{-1}$, where σ_k is the kth singular value of the normalized channel matrix. Median EDOF for all monopole data is given in Table VIII, showing only slight differences between the 2.55 and 24 GHz data and further suggesting adequate multipath for spatial multiplexing at 24 GHz.

VI. CONCLUSION

This paper presents co-located 2.55 and 24 GHz MIMO measurements performed in two indoor environments. The results demonstrate that the channel properties are very similar in the two buildings and further show remarkable similarity in the channels at the low and high microwave frequencies in some cases. Specifically, in hallway environments and in connected labs, the link loss often looks very similar at the two bands after compensating for lost power due to the smaller receive aperture at 24 GHz. For NLOS conditions, the 24 GHz signal suffers from 5 to 20 dB (11 dB average) additional loss compared to that observed at 2.55 GHz. The results also show that in indoor NLOS channels, misaligned directional antennas may cause significant performance degradation (13 dB on average), hlighlighting the need for adaptive arrays. Median RMS delay spreads in the range of 20 to 35 ns were seen at 24 GHz, which is similar to previously reported values at 2.4 GHz. Capacity of a 4×4 system was found to be very similar at 2.55 and 24 GHz, indicating that multipath is still quite rich at 24 GHz in the environments tested.

RT simulations reveal that material loss must increase at 24 GHz to provide a good fit to the measured data, indicating a need for accurate characterization of common building materials at high microwave frequencies. It also appears that modeling furniture, and possibly diffuse effects, may be more critical at 24 GHz than at 2.55 GHz.

The results herein suggest that 24 GHz is a viable option for replacing medium range (10-30 m) NLOS wireless services currently at 2.4 GHz. The main effect of the higher frequency will be the receive aperture loss (20 dB) when small wavelength-scale antennas are used plus an additional 5-20 dB

loss when penetrating walls or propagating around hallway corners.

REFERENCES

[1] V. Visoottiviseth, T. Piroonsith, and S. Siwamogsatham, "An empirical study on achievable throughputs of IEEE 802.11n devices," in *7th Intl. Symp. Modeling Optimization in Mobile, Ad Hoc, and Wireless Networks*, Seoul, South Korea, June 23-27, 2009, pp. 1–6.

[2] N. Mishra *et al.*, "Usage of 802.11n in practice: A measurement study," in *7th Intl. Conf. Commun. Systems and Networks*, Bangalore, India, Jan. 6-10, 2015, pp. 1–8.

[3] OpenSignal, "The state of LTE," OpenSignal, Inc., Tech. Rep., Feb. 2016. [Online]. Available: https://opensignal.com

[4] S. Segan, "Fastest mobile networks 2016," *PC Magazine*, June 2016. [Online]. Available: http://www.pcmag.com

[5] H. Xu, V. Kukshya, and T. S. Rappaport, "Spatial and temporal characteristics of 60-GHz indoor channels," *IEEE J. Selected Areas Commun.*, vol. 20, pp. 620–630, Apr. 2002.

[6] C. R. Anderson and T. S. Rappaport, "In-building wideband partition loss measurements at 2.5 and 60 GHz," *IEEE Trans. Wireless Commun.*, vol. 3, pp. 922–928, May 2004.

[7] N. Moraitis and P. Constantinou, "Indoor channel measurements and characterization at 60 GHz for wireless local area network applications," *IEEE Trans. Antennas Propag.*, vol. 52, pp. 3180–3189, Dec. 2004.

[8] T. Zwick, T. J. Beukema, and H. Nam, "Wideband channel sounder with measurements and model for the 60 GHz indoor radio channel," *IEEE Trans. Veh. Technol.*, vol. 54, pp. 1266–1277, July 2005.

[9] P. F. M. Smulders, "Statistical characterization of 60-GHz indoor radio channels," *IEEE Trans. Antennas Propag.*, vol. 57, pp. 2820–2829, Oct. 2009.

[10] M. Jacob *et al.*, "Diffraction in mm and sub-mm wave indoor propagation channels," *IEEE Trans. Microwave Theory Tech.*, vol. 60, pp. 833–844, Mar. 2012.

[11] W. Fu, J. Hu, and S. Zhang, "Frequency-domain measurement of 60 GHz indoor channels: a measurement setup, literature data, and analysis," *IEEE Instrum. Meas. Mag.*, vol. 16, pp. 34–40, Apr. 2013.

[12] K. Haneda *et al.*, "A statistical spatio-temporal radio channel model for large indoor environments at 60 and 70 GHz," *IEEE Trans. Antennas Propag.*, vol. 63, pp. 2694–2704, June 2015.

[13] J. Pascual-García *et al.*, "On the importance of diffuse scattering model parameterization in indoor wireless channels at mm-wave frequencies," *IEEE Access*, vol. 4, pp. 688–701, Feb. 2016.

[14] S. Geng, J. Kivinen, X. Zhao, and P. Vainikainen, "Millimeter-wave propagation channel characterization for short-range wireless communications," *IEEE Trans. Veh. Technol.*, vol. 58, pp. 3–13, Jan. 2009.

[15] A. Maltsev *et al.*, "Experimental investigations of 60 GHz WLAN systems in office environment," *IEEE J. Selected Areas Commun.*, vol. 27, pp. 1488–1499, Oct. 2009.

[16] T. S. Rappaport, G. R. MacCartney, M. K. Samimi, and S. Sun, "Wideband millimeter-wave propagation measurements and channel models for future wireless communication system design," *IEEE Trans. Commun.*, vol. 63, pp. 3029–3056, Sep. 2015.

[17] G. R. MacCartney, T. S. Rappaport, S. Sun, and S. Deng, "Indoor office wideband millimeter-wave propagation measurements and channel models at 28 and 73 GHz for ultra-dense 5G wireless networks," *IEEE Access*, vol. 3, pp. 2388–2424, Oct. 2015.

[18] A. I. Sulyman *et al.*, "Radio propagation path loss models for 5G cellular networks in the 28 GHz and 38 GHz millimeter-wave bands," *IEEE Communications Mag.*, vol. 52, pp. 78–86, Sep. 2014.

[19] ——, "Directional radio propagation path loss models for millimeter-wave wireless networks in the 28-, 60-, and 73-GHz bands," *IEEE Trans. Wireless Commun.*, vol. 15, no. 10, pp. 6939–6947, Oct. 2016.

[20] J. Lee *et al.*, "Measurement-based propagation channel characteristics for millimeter-wave 5G Giga communication systems," *ETRI Journal*, vol. 38, pp. 1031–1041, Dec. 2016.

[21] X. Wu *et al.*, "28 GHz indoor channel measurements and modelling in laboratory environment using directional antennas," in *Proc. 2015 European Conf. Antennas and Propag.*, Lisbon, Portugal, Apr. 13-17, 2015, pp. 1–5.

[22] D. Lu and D. Rutledge, "Investigation of indoor radio channels from 2.4 GHz to 24 GHz," in *Proc. 2003 IEEE Antennas and Propag. Society Intl. Symp.*, vol. 2, Columbus, OH, June 22-27, 2003, pp. 134–137.

[23] O. J. Femi-Jemilohun, T. Quinlan, S. Barc, and S. D. Walker, "An experimental investigation into GbE wireless data communication at 24 GHz in non-line-of-sight and multipath rich environments," *IEEE Antennas Wireless Propag. Lett.*, vol. 13, pp. 1219–1222, 2014.

[24] O. J. Femi-Jemilohun and S. D. Walker, "Path loss prediction models for corridor propagation at 24 GHz," *Trans. Networks and Commun.*, vol. 2, no. 4, pp. 84–94, 2014.

[25] M. C. Parker, G. Koczian, T. Quinlan, and S. D. Walker, "High capacity communications at 24 GHz and 60 GHz for converged 5G networking," in *European Conf. Networks and Opt. Commun.-(NOC)*, London, UK, June 30 - July 2, 2015, pp. 1–6.

[26] B. T. Maharaj, J. W. Wallace, M. A. Jensen, and L. P. Linde, "A low-cost open-hardware wideband multiple-input multiple-output (MIMO) wireless channel sounder," *IEEE Trans. Instrum. Meas.*, vol. 57, pp. 2283 – 2289, Oct. 2008.

[27] R. Mehmood, J. W. Wallace, and M. A. Jensen, "24 GHz indoor MIMO channel measurements," in *Proc. 2015 IEEE Antennas and Propag. Society Intl. Symp.*, Vancouver, Canada, July 19-24, 2015, pp. 1786–1787.

[28] ——, "LOS and NLOS millimeter-wave MIMO measurements at 24 GHz in a hallway environment," in *Proc. 2016 IEEE Antennas and Propag. Society Intl. Symp.*, Fajardo, Puerto Rico, June 26 - July 1, 2016, pp. 1–2.

[29] G. R. MacCartney, S. Deng, and T. S. Rappaport, "Indoor office plan environment and layout-based mmWave path loss models for 28 GHz and 73 GHz," in *Proc. 2016 IEEE 83rd Veh. Technol. Conf.*, Nanjing, China, May 15-18, 2016, pp. 1–6.

[30] K. Haneda *et al.*, "Indoor 5G 3GPP-like channel models for office and shopping mall environments," in *Proc. 2016 IEEE Intl. Conf. Commun. Workshops*, Kuala Lumpur, Malaysia, May 23-27, 2016, pp. 694–699.

[31] 3GPP, "Study on channel model for frequency spectrum above 6 GHz, Tech. Rep. 38.900 (Release 14), 2016.

[32] O. H. Koymen, A. Partyka, S. Subramanian, and J. Li, "Indoor mm-Wave channel measurements: Comparative study of 2.9 GHz and 29 GHz," in *Proc. 2015 IEEE Global Telecomm. Conf.*, San Diego, CA, Dec. 6-10, 2015, pp. 1–6.

[33] S. h. Min *et al.*, "Spatial and temporal characterization of indoor millimeter wave propagation at 24 GHz," *Intl. J. Antennas Propag.*, pp. 1–10, Sep. 2017.

[34] I. Rodriguez *et al.*, "Analysis and comparison of 24 GHz cmWave radio propagation in urban and suburban scenarios," in *Proc. 2016 IEEE Wireless Commun. and Networking Conf.*, Doha, Qatar, Apr. 3-6, 2016, pp. 1–7.

[35] P. Truffer and P. E. Leuthold, "Wide-band channel sounding at 24 GHz based on a novel fiber-optic synchronization concept," *IEEE Trans. Microwave Theory Tech.*, vol. 49, pp. 692–700, Apr. 2001.

[36] R. Van Nee, "Delay spread requirements for wireless networks in the 2.4 GHz and 5 GHz bands," Nov. 1997, doc: IEEE P802.11-97/125.

[37] M. K. Samimi and T. S. Rappaport, "3-D millimeter-wave statistical channel model for 5G wireless system design," *IEEE Trans. Microwave Theory Tech.*, vol. 64, pp. 2207–2225, July 2016.

[38] D.-S. Shiu, G. J. Foschini, M. J. Gans, and J. M. Kahn, "Fading correlation and its effect on the capacity of multielement antenna systems," *IEEE Trans. Commun.*, vol. 48, pp. 502–513, Mar. 2000.